JOURNAL OF SOLID STATE CHEMISTRY 108, 346–355 (1994)

HREM Study of the 30 K Superconductor $Bi_2Sr_4Cu_2CO_3O_8$

M. Hervieu, M. T. Caldes,* C. Michel, D. Pelloquin, and B. Raveau

*Laboratoire CRISMAT-ISMRA—Université de Caen, Boulevard du Maréchal Juin, 14050 Caen Cedex, France; and *Instituto de Ciencias de Materiales—CSIC, Campus UAB, 08193 Bellaterra, Spain*

Received February 12, 1993; in revised form June 7, 1993; accepted June 9, 1993

The structure and the microstructure of a new high Tc superconductor $Bi_2Sr_4Cu_2CO_3O_8$ have been studied by high-resolution electron microscopy. The [110] orientation allows us to image the layers stacking, and the [010] calculated images allow us to interpret the contrast. The oxycarbonate $Bi_2Sr_4Cu_2CO_3O_8$ exhibits a modulated structure; the mean value of the component of the modulation vector along $\vec{b}$ is 8.85 but this periodicity is not constant. The relative arrangement of the double bismuth layers $[BiO]_2$ involves the periodic compression of the intermediate layer, resulting in a strong variation of the contrast. The existence of additional slices, $[Sr_2CuCO_3O_2]$ or $[Bi_2Sr_2CuO_6]$, suggests the existence of a large family which can be formulated $[Bi_2Sr_2CuO_6]_n\,[Sr_2CuCO_3O_2]_{n'}$; $n' = 1$ to 5, and $n = 1$ and 2 have been observed. The existence of a shearing mechanism along $\vec{c}$ involves the connection of layers of different natures through the boundary; this mechanism is not only observed as isolated defects but can lead to the formation of a new "collapsed oxycarbonate" phase. Other structural features such as the micalike morphology and the existence of 90° oriented domains are discussed. © 1994 Academic Press, Inc.

INTRODUCTION

The recent discovery of two new superconductors $Tl_{0.5}Pb_{0.5}Sr_4Cu_2CO_3O_7$ (1) and $Bi_2Sr_4Cu_2CO_3O_8$ (2) has demonstrated that the mechanism of substitution of CO_3 groups for copper polyhedra, first evidenced in the perovskite structure (3–9), could be generalized to the layered cuprates built up from the alternate stacking of rock salt layers and perovskite-type layers (10). Indeed, these oxycarbonates can be described as a stacking of the $Sr_2CuO_2CO_3$ structure (9) and the 1201 or the 2201 structures. The HREM study of thallium oxycarbonate, $Tl_{0.5}Pb_{0.5}Sr_4Cu_2CO_3O_7$ (11), showed that the stacking of the different layers along the $\vec{c}$ axis is highly regular. In contrast, it is well established that the structures of bismuth cuprates are generally more complex than those of thallium cuprates. The first reason for this complexity is the existence of an incommensurate modulation resulting from modulated displacements and distributions of the ions in the structure. The second difference deals with the existence of several structural families of bismuth cuprates, such as the "collapsed phases" (12, 13), the orthorhombic tubular phases (14–16), and the monoclinic tubular phases (17, 18), closely related to each other from the viewpoint of structure and composition. It was shown by HREM (18) that such phases may exist as extended defects in the layered bismuth cuprates. Similar phenomena can appear in the bismuth oxycarbonate. This paper deals with the HREM study of the 30 K superconductor $Bi_2Sr_4Cu_2CO_3O_8$.

EXPERIMENTAL

As previously reported (2), two different types of synthesis can be used for the preparation of the materials, working either in air at low temperature to avoid a complete decarbonation or in a sealed tube, starting from the stoichiometric composition. The purity of the samples was checked by X-ray diffraction and electron diffraction (ED) techniques.

The ED study was performed with JEOL 120CX and 200CX electron microscopes, fitted with a side entry goniometer. The HREM study was performed with a TOPCON 002B EM operating at 200 kV; the aberration constant of the objective lens is 0.4 mm. The samples were prepared by a smooth splitting of the oxycarbonate grains in *n*-butanol deposited on a holey carbon film supported by aluminium grids. The EDX analysis was performed with a KEVEX analyzer.

Structure Recall

The electron diffraction study (2) allowed us to determine the parameters of the orthorhombic cell which were then refined to the values

$$a = 5.466(2)\ \text{Å},\ b = q \times 5.460(2)\ \text{Å},\ \text{and}\ c = 39.500(9)\ \text{Å}.$$

The structure is modulated along $\vec{b}$, with q ranging from 8.85 to 9. The reflection conditions lead to the space groups *Abmm* or *Abm*2. [001] and [100] electron diffraction patterns are given in Fig. 1.

The best orientation to image the layers stacking in the

0022-4596/94 $6.00

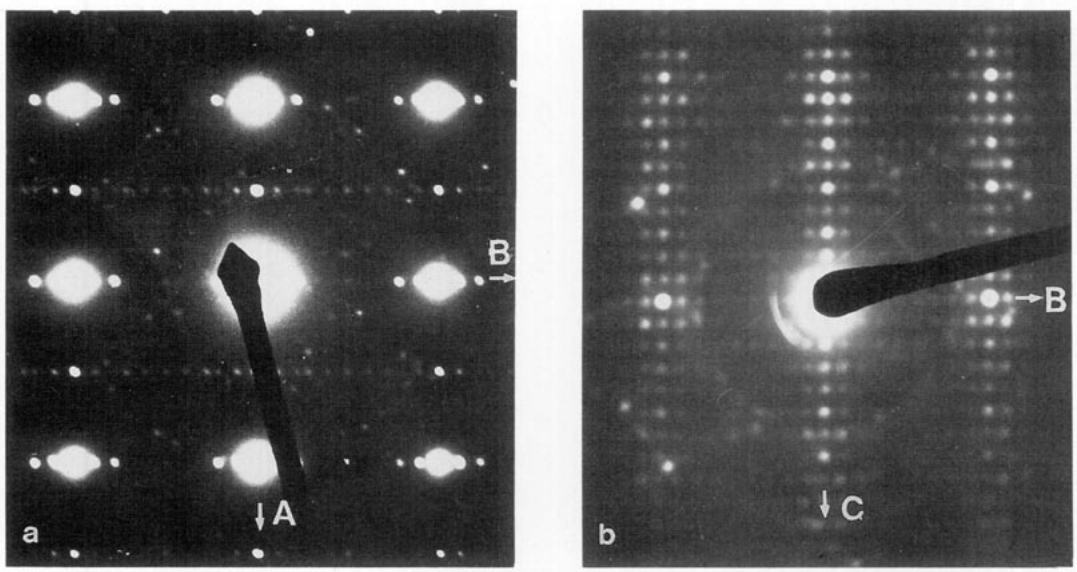

FIG. 1. (a) [001] and (b) [100] electron diffraction patterns of $Bi_2Sr_4Cu_2CO_3O_8$.

layered cuprate is the $[100]_p$ direction of the perovskite subcell, i.e., the [110] direction for our sample. Such an image (Fig. 2a) shows clearly that the sequence of the four layers $[SrO]_\infty[BiO]_\infty[BiO]_\infty[SrO]_\infty$ observed in the bismuth cuprates remains unchanged. However, in the middle of the perovskite slice, a very bright row (see curved arrows) is observed, similar to that observed in the oxycarbonate $Tl_{0.5}Pb_{0.5}Sr_4Cu_2CO_3O_7$ (1); in the latter, this row is correlated to the existence of a carbonate layer. A structural model could thus be proposed (Fig. 2b) which was confirmed by an X-ray diffraction study. The structure is described as the intergrowth of a 2201-type slice, $[Bi_2Sr_2CuO_6]_\infty$ with a single $[Sr_2CuCO_3O_2]_\infty$ layer.

RESULTS AND DISCUSSION

In order to detect the presence of eventual extended defects, the structure was investigated along $[110]_p$, i.e., along [010] and [100]. The most evident contrast of the [010] images results from the presence of bismuth and carbonate layers. An example is shown in Fig. 3, where the [BiO] layers appear as two rows of black dots (black arrows) and the carbonate layer as the brightest row (curved arrows). To confirm this contrast we have calculated images, on the basis of the positional parameters refined from the X-ray data (2). It appears, in agreement with the experimental images, that the $[BiO]_\infty$ and $[CO]_\infty$ layers involve a characteristic contrast all along the through focus series; on the experimental image, with a focus value close to −30 nm, the calculated image is superposed (Fig. 3). Nevertheless some small differences are observed which can be easily explained by the complicated character of this modulated structure:

(i) In the experimental images, the white dots are not as well resolved as in the calculated images. This results from the displacement of the atoms along $\vec{c}$, which is due to the displacing modulation. Such displacements are not taken into consideration in the average structure for image calculations, so that the Sr and Cu columns cannot be resolved. Such a phenomenon was also observed in the bismuth cuprates (19–21).

(ii) The contrast at the level of the bismuth atoms, which are lined up in pairs and not equidistantly spaced, leads to the existence of alternated dark and grey dots. Such a feature was also observed in the bismuth 2212 and 2223 cuprates and was interpreted as a shifting of the Bi atoms along $\vec{a}$ (19).

The Modulation

The oxycarbonate $Bi_2Sr_4Cu_2CO_3O_8$ exhibits a modulated structure, and the displacement of the atoms is easily seen in high-resolution images. Two orientations, [100] and [001], allow us to image this displacing modulation.

The [100] overall image in Fig. 4 shows the spectacular contrast which results from the complex layers stacking along $\vec{c}$ and from the modulation along $\vec{b}$. The corresponding enlarged image in Fig. 5a shows the rows of Bi atoms which appear as white dots; in Fig. 5b the Bi atoms appear as dark rows. In each of these enlarged images the rows of carbonate groups exhibit the opposite contrast (see curved arrows). From these images, the undulation of the atomic layers, which governs the displacing modulation along $\vec{b}$, is clearly visible. One observes (Fig. 5a) that two successive $[BiO]_\infty$ layers forming the bismuth bilayers are waving in antiphase, as in the 2212 and 2223 bismuth

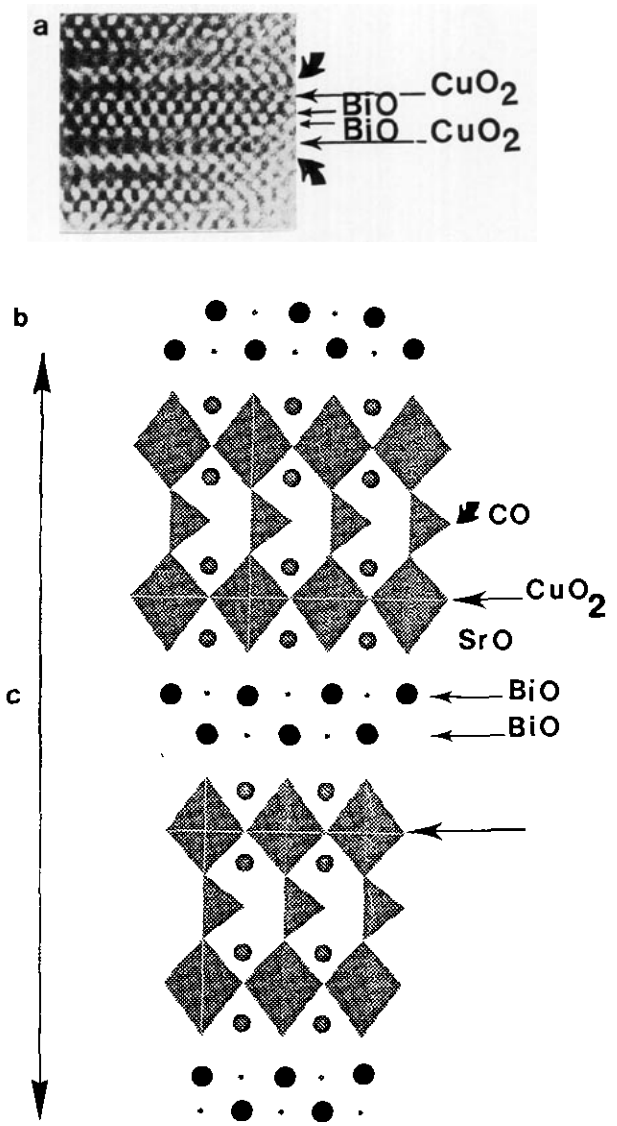

FIG. 2. (a) [110] HREM image which shows the layers stacking along $\vec{c}$. Carbonate layers are represented by curved arrows; (b) idealized model of the structure projected along [1$\bar{1}$0].

cuprates (Fig. 6). Nevertheless the modulation patterns are basically different from the bismuth cuprates, since two successive bismuth bilayers $[(BiO)_2]_\infty$ are waving in phase in the oxycarbonate (Fig. 6a), whereas they are waving in antiphase in the bismuth cuprates (Fig. 6b).

The periodicity along $\vec{b}$, resulting from the displacing modulation, is not constant from one cell to the adjacent ones; some local variations are observed, with q varying from 6 to 10. Two examples are shown in Fig. 7. In the first [100] image (Fig. 7a) we observe the following sequence for the q value: 7–10–9–9. The second micrograph is a [001] image (Fig. 7b); along that orientation, the q value can also easily be imaged and an aleatory sequence of 7, 8, 9, and 10 q value can be observed in that part of the crystal.

The relative arrangement, in phase, of two adjacent double bismuth layers and the amplitude of the atomic displacement implies that the intermediate layer, where the carbonate groups are located, is sandwiched between two $[SrO]_\infty$ layers which undulate in phase. As a result, this intermediate layer is periodically compressed. The contrast at the level of this layer varies so strongly that it is impossible to establish whether the phenomenon is correlated to a modulated replacement of carbonate groups by a foreigner atom (copper or bismuth) or is the only consequence of the atomic displacements.

Oriented Domains

Domains with 90° orientation are sometimes observed in the crystals; a typical [001] ED pattern is shown in Fig. 8a where the b_1 and b_2 axes of the domains are perpendicularly oriented. The corresponding bright field image (Fig. 8b) shows that the domains exhibit a boundary parallel to (110). Note that such an arrangement of the oriented domains (Fig. 8c) is different from that observed in the bismuth cuprates where the 90° oriented slices are always

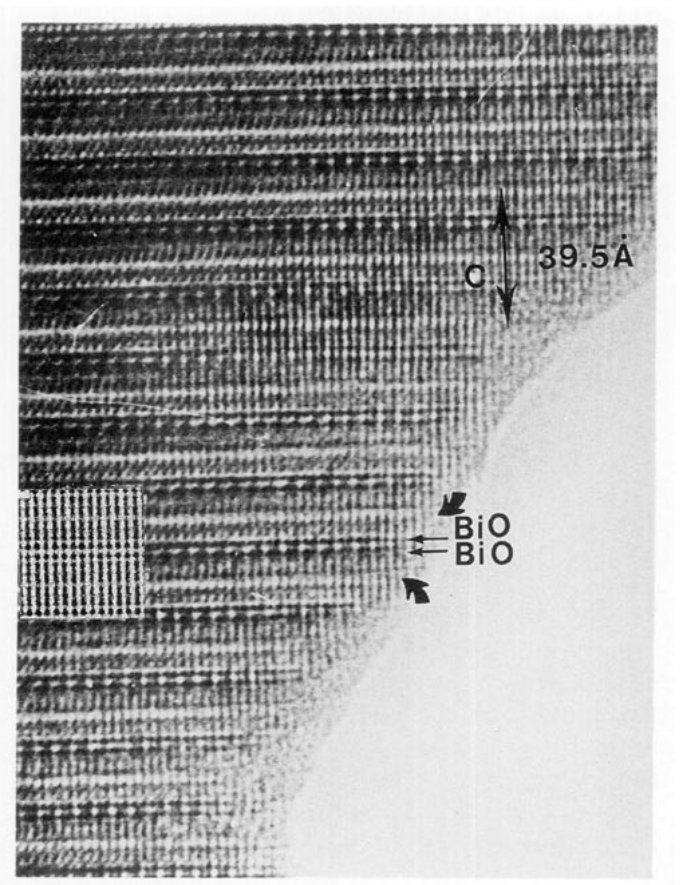

FIG. 3. [010] HREM image of $Bi_2Sr_4Cu_2CO_3O_8$. [BiO] layers are shown by black arrows and the [CO] layers by curved arrows. The calculated image for $\Delta f = -30$ nm is superposed.

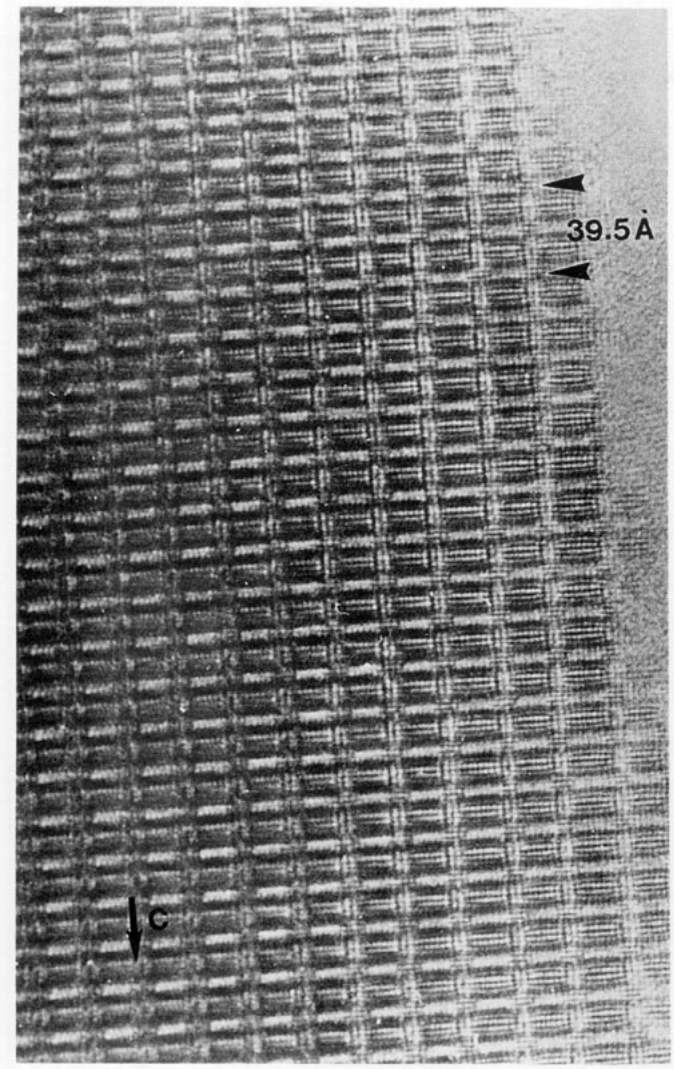

FIG. 4. Overall [100] image.

superposed along $\vec{c}$, with a boundary parallel to (001) (Fig. 8d).

Intergrowth Defects: The Members $(Bi_2Sr_2CuO_6)_n(Sr_2CuO_2CO_3)_{n'}$

The description of $Bi_2Sr_4Cu_2CO_3O_8$ (2) as the first member of a series of intergrowth of the two structures 2201 and $Sr_2CuO_2CO_3$ with the generic formula $(Bi_2Sr_2CuO_6)_n$ $(Sr_2CuO_2CO_3)_{n'}$ (Fig. 2b) suggests the existence of stacking defects along $\vec{c}$ corresponding to a variation of the thickness either of the $Sr_2CuO_2CO_3$-type slices or of the $Bi_2Sr_2CuO_6$-type slices.

Extra $Sr_2CuO_2CO_3$ *Slices: The Defects* $(Bi_2Sr_2CuO_6)(Sr_2CuO_2CO_3)_{n'}$

Two examples of the introduction of additional $Sr_2CuO_2CO_3$-type slices are shown in Fig. 9. The first example deals with the [110] image of such a crystal (Fig. 9a), where the carbonate layers are imaged as rows of bright dots; it shows at the level of the defect (middle part of the image) two adjacent bright rows separated by one row of grey dots. The latter is correlated to a copper layer so that this defect corresponds to the local sequence Bi–Sr–Cu–Sr–C–Sr–Cu–Sr–C–Sr–Cu–Sr–Bi. Thus this defect can be represented as the local stacking of a single 2201 layer with a double $Sr_2CuO_2CO_3$ layer (Fig. 9b) according to the formulation $(Bi_2Sr_2CuO_6)$ $(Sr_2CuO_2CO_3)_2$ $(n = 2)$. The periodicity of the defect along $\vec{c}$, close to 54.2 Å, is in agreement with the sum of the different thicknesses of the slices.

The second example, observed from a [010] image (Fig. 9c), shows the variation of the thickness of the Sr_2CuO_2-CO_3-type layers, i.e., of n', in an aleatory way. The carbonate layers are also imaged as rows of bright dots, and we observe sequences of 2, 3, 4, and 5 bright rows separated by one row of grey dots. The formulation of these new members is $[Bi_2Sr_2CuO_6][Sr_2CuO_2CO_3]_{n'}$, with n' ranging from 1 to 5.

Extra $[Bi_2Sr_2CuO_6]$ *Slices*

Additional $[Bi_2Sr_2CuO_6]_\infty$ layers are also observed in the crystals. In the overall [100] images (Fig. 10a), two isolated defects are indicated by black arrowheads; they correspond to the formation of two adjacent $[Bi_2Sr_2CuO_6]$ units, corresponding to the local intergrowth $(Bi_2Sr_2$ $CuO_6)_2(Sr_2CuO_2CO_3)$, i.e., $n = 2$ and $n' = 1$ (Fig. 10b). The local periodicity along $\vec{c}$ is 64.1 Å. The two intergrowth units, $[Bi_2Sr_2CuO_6]$ and $[Bi_2Sr_4Cu_2CO_3O_8]$, are modulated but with different q values, $q \sim 5$ and $q \sim 9$, respectively. The difference between these values implies

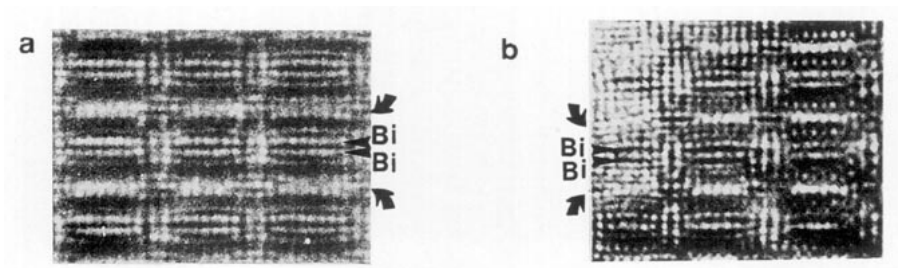

FIG. 5. Enlarged images where the bismuth layers are imaged as (a) rows of white dots and (b) dark rows.

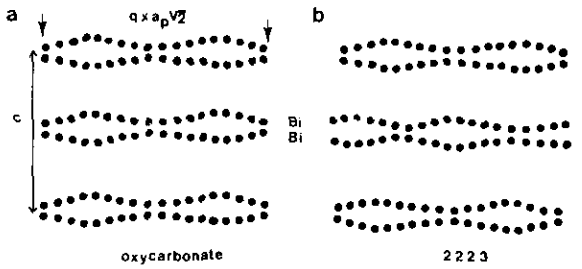

FIG. 6. Idealized representation of the modulation patterns of the double bismuth layers. Two adjacent double layers are in phase in the oxycarbonate (a), whereas they are out of phase in the oxide 2223 (b).

that the modulations of the two oxycarbonate zones which sandwich the additional 2201 unit are shifted; this is clearly observed in Fig. 10a.

In the same image, a very thick slice of the 2201 structure, corresponding to the local intergrowth $(Bi_2Sr_2CuO_6)_7$ $(Sr_2CuO_2CO_3)$ is observed (curved arrow at the bottom of the micrograph in Fig. 10a). Such a defect is quite rare.

These observations confirm the possibility of building new phases with the generic formula $(Bi_2Sr_2CuO_6)_n(Sr_2CuO_2CO_3)_{n'}$, the present phase $Bi_2Sr_4Cu_2CO_3O_8$ being the first member of the series ($n = n' = 1$).

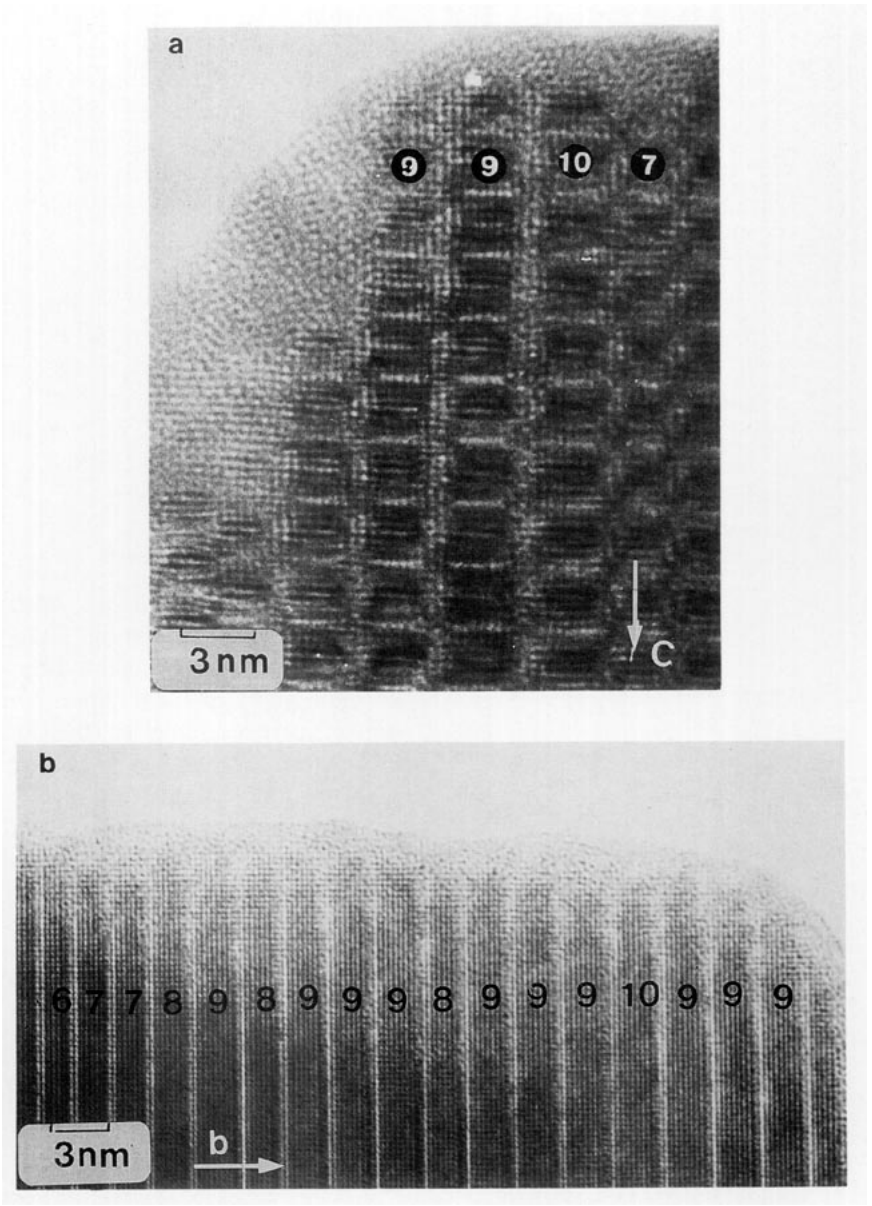

FIG. 7. Variations of the periodicity along $\vec{b}$ observed along (a) [100] and (b) [001].

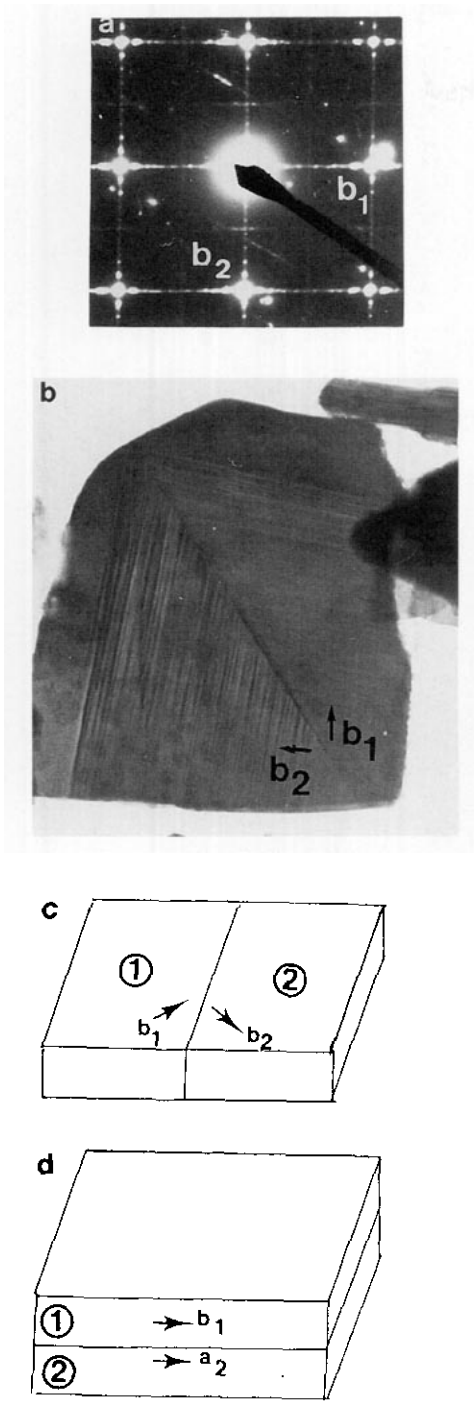

FIG. 8. Existence of oriented domains. (a) Typical [001] ED pattern and (b) bright field image. The boundary is parallel to (110). Schematical representation of the oriented domains in (c) and oxycarbonate and (d) the 2223 type oxide.

Additional SrO Layers

Besides the above intergrowth defects, a third type of defect corresponding to the appearance of additional layers, probably SrO, at the level of the rock salt layers (Fig. 11) is also observed. One observes a highly disordered zone some 10 Å wide, which separates the crystal into thin lamellae. Moreover the thickness of the ill crystallized slice varies, involving a slight disorientation of the two adjacent lamellae.

Note also the micalike morphology of the crystal, which is as pronounced as in the bismuth cuprates; as for the latter, the cleavage is usually observed between two $[BiO]_\infty$ layers (Fig. 11).

Collapsed Defects

Shearing of the structure along $\vec{c}$ sometimes appears right through the crystals as shown on the enlarged image of Fig. 12a. One observes that the $[BiO]_\infty$ layers (dark rows) are translated along $\vec{c}$ with respect to the carbonate layers (rows of bright dots) on each side of the boundary (see large arrows). As a result, layers of different natures are connected through this boundary. As shown from the idealized structural model (Fig. 12b), in the bismuth bilayers, one of the $[BiO]_\infty$ layers is connected to a carbonate layer, whereas the second one is connected to a $[SrO]_\infty$ layer in a systematic way. Similarly, one $[SrO]_\infty$ layer is connected to a copper layer, whereas the other layers remain unchanged through the boundary.

Such a phenomenon which involves the connection of layers of different natures was observed in the collapsed phases $Bi_{17}Sr_{16}Cu_7O_{39}$ (12, 13), $Bi_{15}Ba_7Sr_7Cu_6O_{42}$ (22), and $Bi_6Ba_4Cu_2O_{15}$ (23); it was also observed as a generator of defects in the tubular phases (16–18). In these examples, the BiO layers are connected either to [SrO] layers or to $[CuO_2]$ layers. This behavior is similar to the shearing mechanism observed for the 62 K superconductor $TlBa_2Sr_2Cu_2CO_3O_8$ (24), characterized by a connection of $[TlO]_\infty$ layers with carbonate layers. Nevertheless in the thallium oxycarbonate the copper layers are never interrupted contrary to the bismuth phase.

This mechanism is not only observed as isolated defects but can lead, in some parts of the crystal, to the formation of large areas, as shown in Fig. 12c. Although this part of the crystal is thick, the rows of carbonate groups appear as white segments. The translation of these rows is then clearly observed in the overall domain. It can be seen that the thickness of the members along the $\vec{b}$ direction is smaller than in the oxycarbonate with an average q value of 7; however, these values vary in the crystal.

The phase which is stabilized in this domain can be called a "collapsed oxycarbonate." Its structure can be described as built up from the alternate stacking along $\vec{c}$ of one $[Bi_2Sr_2CuO_6]$ slice and a $[Sr_2CuCO_3O_2]$ layer; these $[Bi_2Sr_4Cu_2CO_3O_8]$ units are translated along $\vec{c}$ every seven octahedra through a shearing mechanism. The formulation may be very close to that of the parent structure $Bi_2Sr_4Cu_2CO_3O_8$, since only the atoms located at the level of the junction are liable to be substituted (22).

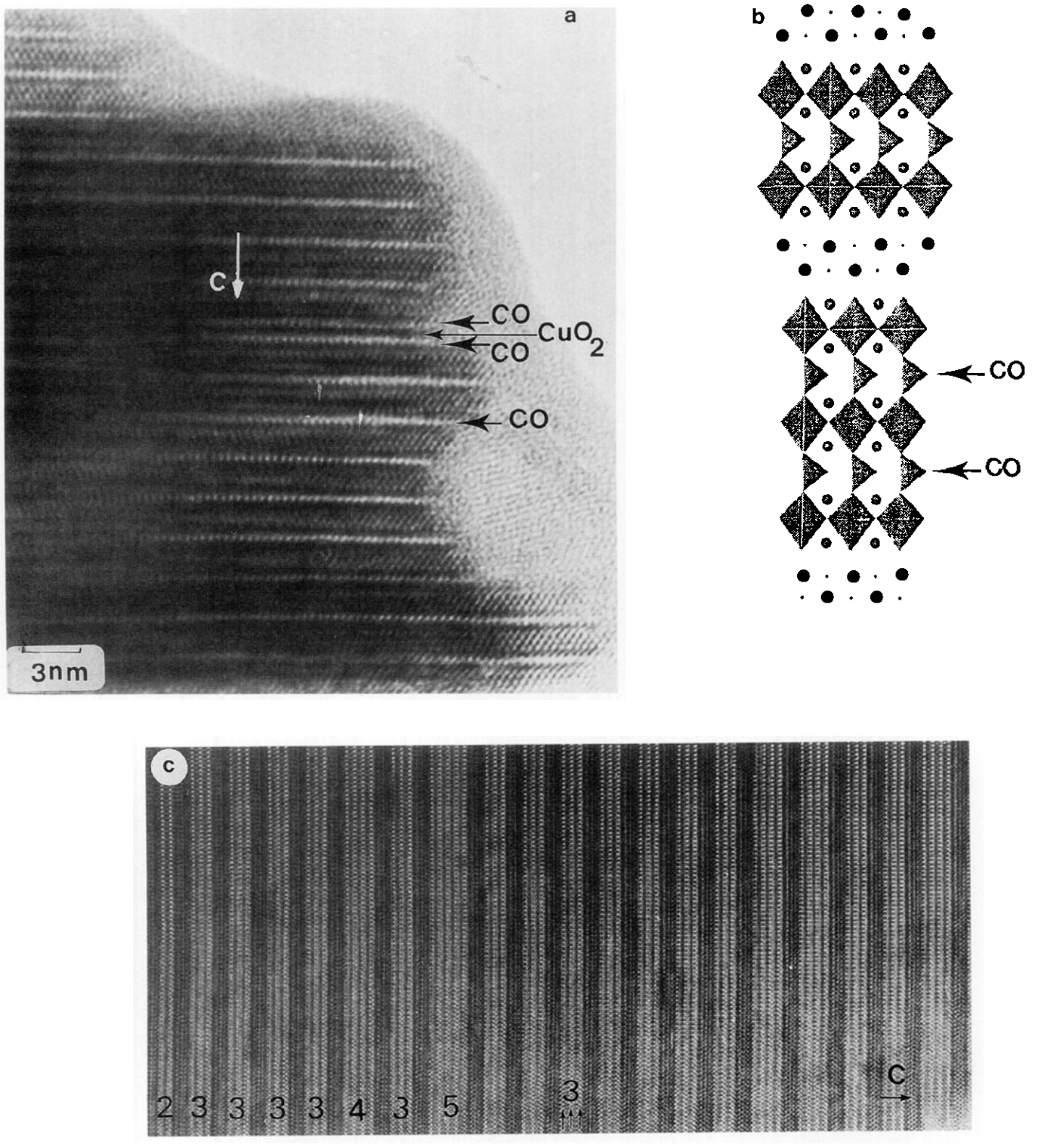

FIG. 9. (a) [110] HREM showing the existence of an extra $[Sr_2CuCO_3O_2]_\infty$ slice and (b) idealized drawing of the defect. (c) [010] HREM image of a crystal where several extra $[Sr_2CuCO_3O_2]_\infty$ slices are observed. The numbers at the bottom indicate the number of adjacent $[Sr_2CuCO_3O_2]$ slices.

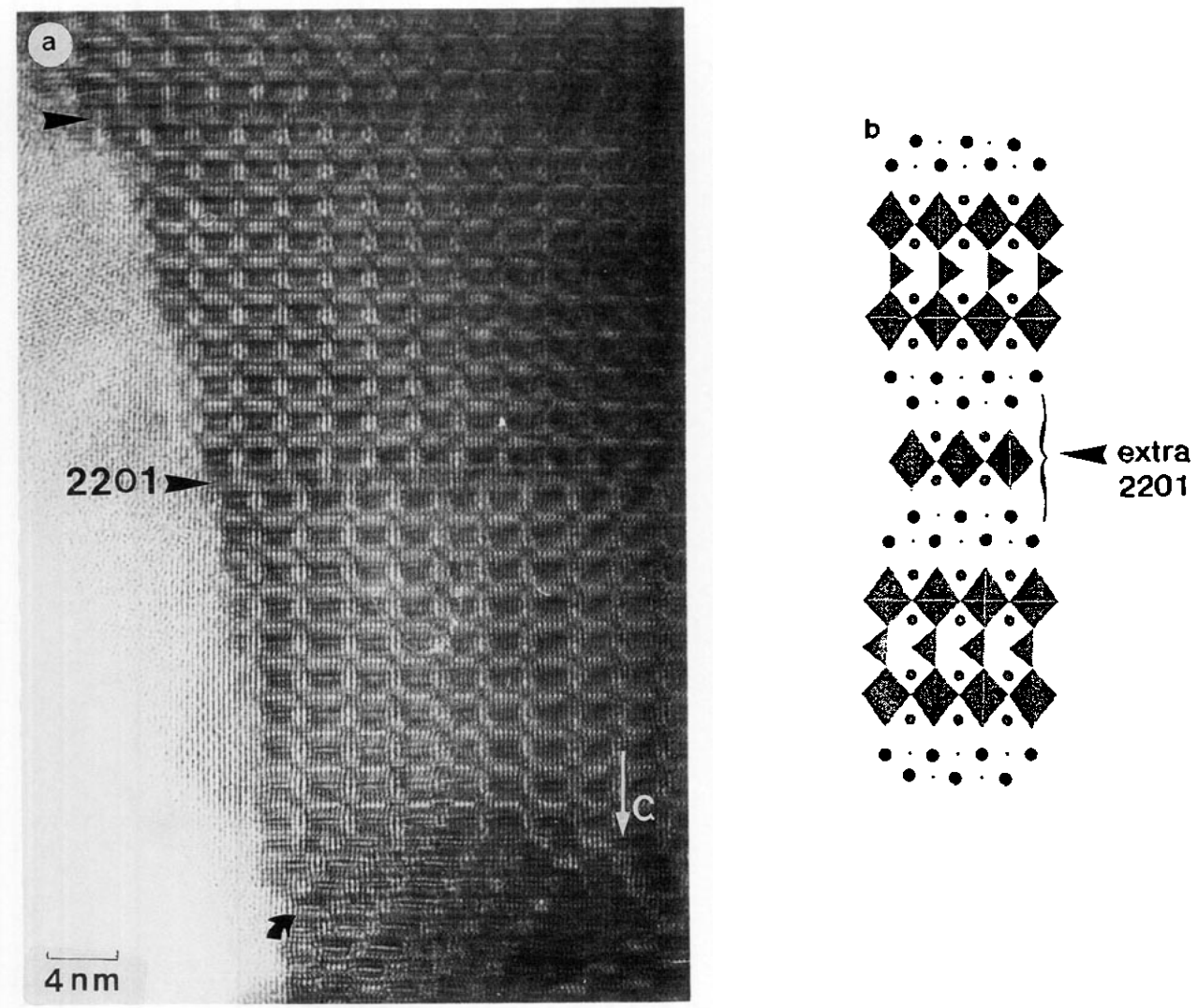

FIG. 10. (a) Overall [100] image where two extra $[Bi_2Sr_2CuO_6]_\infty$ layers are observed as isolated defects (black arrowheads) and (b) idealized drawing of the defect.

Note that in this "collapsed oxycarbonate" structure some defects are observed. It is shown by a white arrow in Figure 12c and corresponds to the disappearance of the white segments correlated with the carbonate group, probably due to a substitution of CO_3 groups by bismuth or copper.

CONCLUDING REMARKS

The HREM investigation of the microstructure of the 30 K superconductor $Bi_2Sr_4Cu_2CO_3O_8$ shows that this system is extraordinarily rich for the generation of new oxycarbonates, superconductive or not. The detection of intergrowth defects confirms the potentiality of these systems for the synthesis of new phases with the generic formula $(Bi_2Sr_2CuO_6)_n(Sr_2CuO_2CO_3)_{n'}$. In the same way, the observation of collapsed defects makes us think that collapsed phases similar to those observed in bismuth cuprates should be generated.

This study also shows the complexity of this structure owing to the problems of modulation, which is variable (ranging from 7 to 9) and probably results from the combination of atomic displacements and substitutions, especially at the level of the carbonate layers.

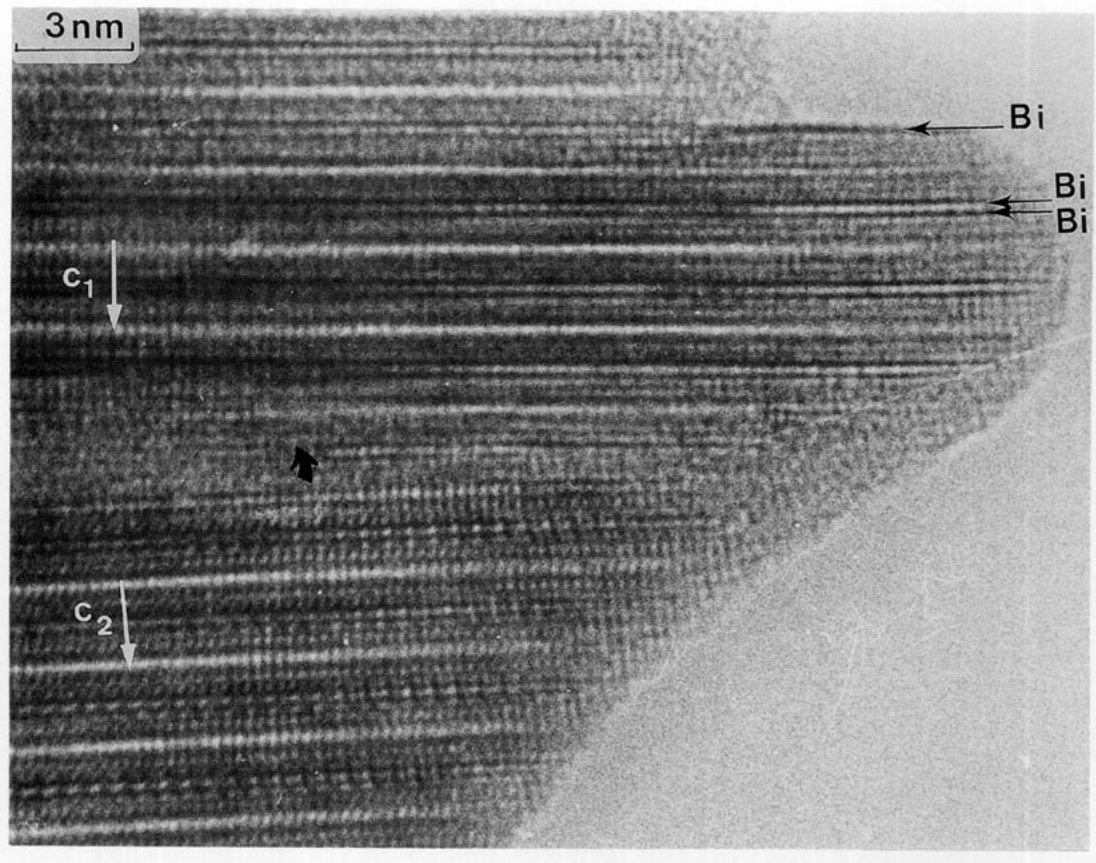

FIG. 11. In some parts of the crystals, additional [SrO] layers are observed. They often involve the formation of highly disordered zones. Note that the two lamellae are slightly misoriented as shown from the c_1 and c_2 axes. The cleavage of the crystal is often observed between the two [BiO] layers as in the bismuth oxide.

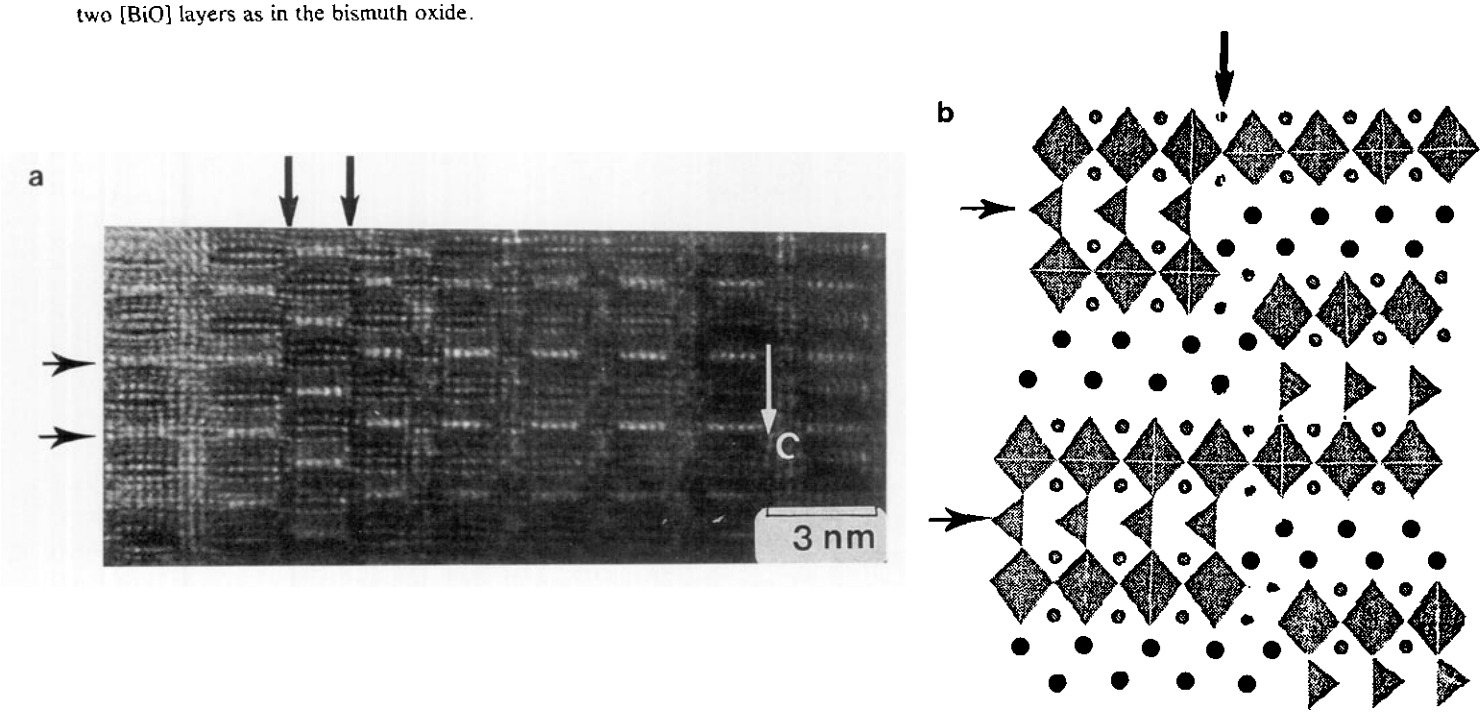

FIG. 12. (a) [100] HREM image where a double shearing mechanism is observed along $\vec{c}$ (big black arrows). The carbonate rows appear as white segments. (b) Idealized model of the defect showing the connection of the different layers through the boundary. (c) Example of a zone where the shearing mechanism is periodically established. The translation of the carbonate segment is clearly observed. The unmarked white arrow indicates the local disappearance of the contrast correlated to the presence of carbonate groups.

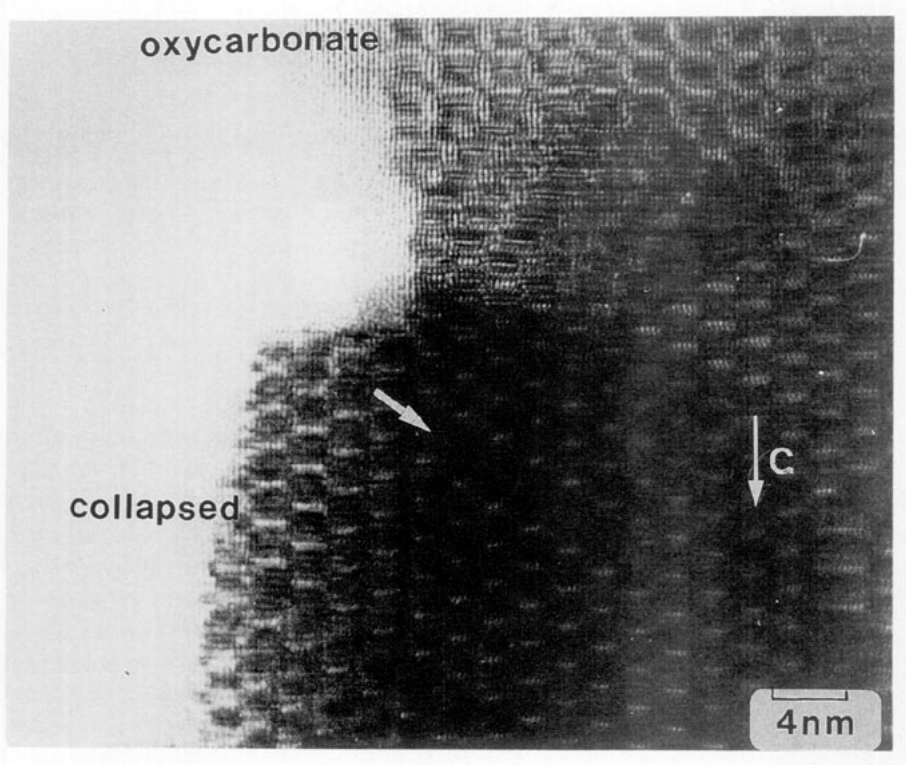

FIG. 12—*Continued*

REFERENCES

1. M. Huvé, C. Michel, A. Maignan, M. Hervieu, C. Martin, and B. Raveau, *Physica C* **205,** 219 (1993).
2. D. Pelloquin, M. Caldes, A. Maignan, C. Michel, M. Hervieu, and B. Raveau, *Physica C* **208,** 121 (1993).
3. C. Greaves and P. R. Slater, *Physica C* **175,** 172 (1991).
4. Y. Miyazaki, H. Yamane, T. Kajitani, T. Oku, K. Hiraga, Y. Morii, S. Funahashi, and T. Hirai, *Physica C* **198,** 7 (1992).
5. F. Izumi, K. Kinoshita, Y. Matsui, K. Yanagisawa, T. Ishigaki, T. Kamiyama, T. Yamada, and H. Asano, *Physica C* **196,** 227 (1992).
6. A. R. Armstrong and P. P. Edwards, *J. Solid State Chem.* **98,** 432 (1992).
7. J. Akimitsu, M. Vehara, M. Ogawa, K. Tomimoto, Y. Miyazaki, H. Yamane, T. Hirai, K. Kinoshita, and Y. Matsui, *Physica C* **201,** 320 (1992).
8. M. Hervieu, Ph. Boullay, B. Domengès, A. Maignan, and B. Raveau, submitted.
9. Y. Miyazaki, H. Yamane, T. Kahjitani, T. Oku, K. Hiraga, Y. Morii, K. Fuchisaki, S. Funahashi, and T. Hirai, *Physica C* **191,** 434 (1992).
10. B. Raveau, C. Michel, and M. Hervieu, *Solid State Ionics* **32–33** 1035 (1989).
11. M. Hervieu, C. Michel, M. Huvé, C. Martin, A. Maignan, and B. Raveau, submitted.
12. Z. Hiroi, Y. Ikeda, M. Takano, and Y. Bando, *J. Mater. Res.* **6,** 435 (1991).
13. Y. Matsui, S. Takekawan, K. Kishio, A. Umezono, S. Nakamura, C. Tsuruta, and K. Ibe, *Mater. Trans.* **31,** 585 (1990).
14. A. Fuertes, C. Miravitlles, J. Gonzalez-Calbert, M. Vallet-Regi, and J. Rodriguez Carvajal, *Physica C* **157,** 529 (1989).
15. M. T. Caldes, J. M. Navarro, F. Perez, M. Carrera, J. Foncuberta, M. Casan-Pastor, C. Miravitlles, X. Obradors, J. Rodriguez-Carvajal, J. M. Gonzalez-Calbert, M. Vallet-Regi, A. Garcia, and A. Fuertes, *Chem. Mater* **3,** 844 (1991).
16. M. T. Caldes, M. Hervieu, A. Fuertes, and B. Raveau, *J. Solid State Chem.* **97,** 48 (1992).
17. M. T. Caldes, M. Hervieu, A. Fuertes, and B. Raveau, *J. Solid State Chem.* **98,** 301 (1992).
18. M. T. Caldes, M. Hervieu, A. Fuertes, and B. Raveau, *J. Solid State Chem.* **98,** 48 (1992).
19. O. Eibl, *Physica C* **168,** 215 (1990).
20. Y. Matsui, S. Takekawa, H. Nozaki, A. Umezono, E. Takayama-Muromachi, and S. Moruichi, *J. Appl. Phys.* **27,** L1241 (1988).
21. H. W. Zandbergen, W. A. Groen, F. C. Mijhoff, G. Van Tendeloo, and S. Amelinckx, *Physica C* **156,** 325 (1988).
22. M. Hervieu, C. Michel, A. Q. Pham, and B. Raveau, *J. Solid State Chem.* **104,** 289 (1993).
23. M. Hervieu, C. Michel, M. T. Caldes, A. Q. Pham, and B. Raveau, *J. Solid State Chem.* **107,** 117 (1993).
24. F. Goutenoire, M. Hervieu, A. Maignan, C. Michel, C. Martin, and B. Raveau, *Physica C* **210,** 359 (1993).